Supplementary Information for "Direct generation of time-energy-entangled W triphotons in atomic vapor"

Kangkang Li[1,5], Jianming Wen[2*], Yin Cai[1*], Saeid Vashahri Ghamsari[2], Changbiao Li[1], Feng Li[1], Zhaoyang Zhang[1], Yanpeng Zhang[1*], and Min Xiao[3,4]

[1]Key Laboratory for Physical Electronics and Devices of the Ministry of Education & Shaanxi Key Lab of Information Photonic Technique, Xi'an Jiaotong University, Xi'an 710049, China

[2]Department of Physics, Kennesaw State University, Marietta, Georgia 30060, USA

[3]National Laboratory of Solid State Microstructures, College of Engineering and Applied Sciences and School of Physics, Nanjing University, Nanjing 210093, China

[4]Department of Physics, University of Arkansas, Fayetteville, Arkansas 72701, USA

[*]emails: jianming.wen@kennesaw.edu; caiyin@xjtu.edu.cn; ypzhang@mail.xjtu.edu.cn.

I. Theory of Time-Energy-Entangled W Triphoton Generation in an Atomic Vapor

– Qualitative Derivation of Fifth-Order Nonlinear Susceptibility $\chi^{(5)}$

– Qualitative Derivations of Linear Susceptibilities χ

– Derivation of the Triphoton W State $|\Psi\rangle$

– Derivations of Temporal Correlations of W Triphotons

– Triphoton W State Entangled in Other Degrees of Freedom

II. Further Information on Experimental Measurements and Data Processing

– Possible Biphoton Processes

– Measured Coincidence Counts by Subtracting Background Accidentals

– Reconstruction Procedure for Triphoton Coincidence Counts

– Additional Experimental Data

III. Comparison of Various Mechanisms on Multiphoton Generation

IV. Further Discussion on the Reported Triphoton Source

References

I. Theory of Time-Energy-Entangled W Triphoton Generation in an Atomic Vapor

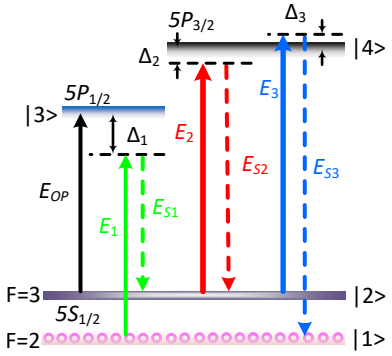

Figure S1 | Energy-level diagram of hot ^{85}Rb atoms for direct generation of time-energy-entangled W-class triphotons. The light-atom interaction in a four-level triple-Λ-type atomic configuration where the two ground states are denoted by $|1\rangle$ and $|2\rangle$, and the two excited states by $|3\rangle$ and $4\rangle$. Initially, all

atomic population is prepared at $|1\rangle$. To ensure no residual atomic population to be distributed in $|2\rangle$, an additional optical pumping beam E_{OP} is applied resonantly with the atomic transition $|2\rangle \leftrightarrow |3\rangle$. A weak pump laser E_1 is applied to $|1\rangle \rightarrow |3\rangle$ with a large, fixed red frequency detuning Δ_1, along with the simultaneous presence of another two strong control fields E_2 and E_3 applied to the same atomic transition $|2\rangle \rightarrow |4\rangle$ but with different frequency detunings Δ_2 and Δ_3. Under the demanded phase-matching conditions, the occurrence of the spontaneous six-wave mixing (SSWM) process will then enable the direct, efficient emission of continuous-mode time-energy-entangled W-type triphotons E_{S1}, E_{S2} and E_{S3} from their respective atomic transitions as schematically sketched in the diagram.

Qualitative Derivation of Fifth-Order Nonlinear Susceptibility $\chi^{(5)}$

Nonlinear optics is a cornerstone for generating, manipulating, and converting quantum light. When an atomic ensemble is utilized to generate nonclassical light, its optical response including both linear and nonlinear susceptibilities can play a decisive role in determining the properties of the produced quantum state and waveform. This is especially true when the light-atom interaction takes place near atomic resonance and the generated nonclassical light is much weaker than the input driving fields. As such, the primary task of this type of problems is to derive the linear and nonlinear susceptibilities for the participating electromagnetic (EM) fields. We notice that when only one EM field is involved per atomic transition, there are several ways such as density-matrix formalism and master equations to compute these susceptibilities. However, the situation becomes exceedingly complicated when more than one optical field acts onto the same atomic transition. For such a case, Wen and his coworkers have developed a useful methodology [1-3] which enables precise calculations on these susceptibilities. While this approach [1-3] in principle allows accurate calculations on optical responses, especially for the production of entangled paired photons, it becomes computationally cumbersome when applied to the triphoton generation considered in this work. We are currently working on the exact derivations using this method. But here we would like to use a qualitative means to study the triphoton emission as well as the associated optical properties. This qualitative method has previously been applied to some atomic systems with similar energy-level structures and coupling interactions [4-8] to ascribe six-wave mixing (SWM). As shall be shown below, despite the derived qualitative results cannot perfectly match the experimental data, they do provide a somewhat plausible explanation for the triphoton formation.

The underlying physics behind this qualitative method is rooted in the perturbation theory, which largely takes into account the dressing steady states but ignores the transient propagation effect. The first step is to perturbatively analyze the SWM process under the weak-field approximation. Then, the dressing perturbation is adopted to set up a set of the strong-field coupled equations to obtain the density-matrix elements through the perturbation chain rule. By following the similar calculations presented in Refs. [4-8], we found that the fifth-order nonlinear susceptibility $\chi^{(5)}$ can be approximately attained from the following perturbation chain,

$$\rho_{11}^{(0)} \xrightarrow{\omega_1} \rho_{31}^{(1)} \xrightarrow{\omega_{S1}} \rho_{21}^{(2)} \xrightarrow{\omega_2} \rho_{41}^{(3)} \xrightarrow{\omega_{S2}} \rho_{11}^{(4)} \xrightarrow{\omega_3} \rho_{41}^{(5)}, \tag{S1}$$

where ω_1, ω_2 and ω_3 are the three input laser frequencies, and ω_{S1}, ω_{S2} and ω_{S3} are generated triphoton frequencies, respectively. By solving the series of density-matrix equations, one can find the density-matrix elements $\rho_{11}^{(0)}$, $\rho_{31}^{(1)}$, …, $\rho_{41}^{(5)}$ in Eq. (S1) step by step. For an atomic vapor, it is necessary to take into account the Doppler broadening effect. After some lengthy calculations, we finally got the fifth-order nonlinear susceptibility of the light-atom interaction displayed in Fig. S1, which has the form of

$$\chi^{(5)}(\delta_2,\delta_3)=\int_{-\infty}^{\infty}dv\frac{2N\mu_{13}\mu_{24}\mu_{23}\mu_{14}^3 f(v)}{\varepsilon_0\hbar^5\left\{\begin{matrix}(\Gamma_{31}+i\Delta_{D1})[(\Gamma_{21}+iW_{D-}\delta_2+iW_{D+}\delta_3)(\Gamma_{41}+iW_{D-}\delta_2+iW_{D+}\delta_3+i\Delta_{D2})+|\Omega_2|^2]\\ \times[(\Gamma_{11}+iW_{D+}\delta_3)(\Gamma_{41}+iW_{D+}\delta_3+i\Delta_{D3})+|\Omega_3|^2]\end{matrix}\right\}}. \quad \text{(S2)}$$

Here, $f(v)=\sqrt{\frac{m_{\mathrm{Rb}}}{2\pi k_B T}}e^{-\frac{m_{\mathrm{Rb}}v^2}{2k_B T}}$ is the Maxwell-Boltzmann velocity distribution of the Rb atoms in thermal motion, where m_{Rb} is the mass of the Rb atom, k_B is the Boltzmann constant, T is the vapor temperature, and v is the atomic kinetic velocity; N denotes the atomic density; μ_{ij} $(i,j=1,2,3,4)$ represents the electric dipole matrix element for the atomic transition $|i\rangle\rightarrow|j\rangle$; ε_0 stands for the vacuum permittivity; Γ_{ij} is the decay or decoherence rate between levels $|i\rangle$ and $|j\rangle$; $\Delta_{D1}=\Delta_1+v\omega_{31}/c$, $\Delta_{D2}=\Delta_2-v\omega_{42}/c$, and $\Delta_{D3}=\Delta_3+v\omega_{42}/c$ with frequency detunings $\Delta_1=\omega_{31}-\omega_1$, $\Delta_2=\omega_{42}-\omega_2$, $\Delta_3=\omega_{42}-\omega_3$, and ω_{ij} being the frequency difference between $|i\rangle$ and $|j\rangle$; $W_{D\pm}=1\pm v/c$ with c the speed of light in vacuum; Ω_2 and Ω_3 are the Rabi frequencies; δ_2 and δ_3 define the spectral distributions with respect to the central frequencies of the emitted E_{S2} and E_{S3} photons, respectively. Owing to the energy conversation in SSWM, the triggers of these two photons require the detection of the output E_{S1} photon at frequency $\omega_{S1}=\omega_1+\omega_2+\omega_3-\omega_{S2}-\omega_{S3}$, which alternatively implies the spectral distributions of the entangled three-photon state to satisfy the condition of $\delta_1+\delta_2+\delta_3=0$. We notice that when $T=80$°C, the Doppler width is estimated to be about $\Delta_D=555$ MHz, orders of magnitude larger than the Rb natural linewidth; the atomic density is $N=1.2\times10^{11}$ cm^{-3}; the optical depth (OD), $OD=N\sigma_{41}L$, has a value of 4.6, where $\sigma_{41}=\frac{\omega_{41}|\mu_{14}|^2}{2\varepsilon_0\hbar c\Gamma_{41}\Delta_D}=3\pi N\Gamma_{41}c^2L/2\Delta_D\omega_{41}^2$ is the on-resonance absorption cross-section of the transition $|1\rangle\rightarrow|4\rangle$. When $T=115$°C, the OD grows to the value of 45.7.

In accordance wtih our previous theoretical studies [1-16], the temporal correlations of the generated triphotons are expected to be governed by two folds of factors: one is the spectral profile of the fifth-order nonlinear susceptibility $\chi^{(5)}$ given in Eq. (S2) and the other is the longitudinal phase-mismatch function (which shall be discussed subsequently). Therefore, we first look at the structure of $\chi^{(5)}$. Similar to our previous analysis [1-15], the resonances arising from the denominator of $\chi^{(5)}$ in Eq. (S2) are centered around $\delta_{1\pm}=\left(\Delta_{D2}\pm\Omega_{E_2}\right)/2(1-\frac{v}{c})$, $\delta_{2\pm\pm}=\left(\Delta_{D3}-\Delta_{D2}\pm\Omega_{E_2}\pm\Omega_{E_3}\right)/2(1+\frac{v}{c})$, and $\delta_{3\pm}=\left(-\Delta_{D3}\pm\Omega_{E_3}\right)/2(1-\frac{v}{c})$, where the effective Rabi frequencies are redefined as $\Omega_{E_2}=\sqrt{{\Delta_{D2}}^2+4|\Omega_2|^2+4\Gamma_{21}\Gamma_{41}}$ and $\Omega_{E_3}=$

$\sqrt{{\Delta_{D3}}^2 + 4|\Omega_3|^2 + 4\Gamma_{11}\Gamma_{41}}$ with Ω_2 and Ω_3 being the original Rabi frequencies of the E_2 and E_3 fields, respectively. The effective linewidths of these resonances are determined by the imaginary parts of the denominator, which are found to be $\Gamma_{\delta_2} = \frac{\Gamma_{21}+\Gamma_{41}}{2} + \frac{\Gamma_{21}\Delta_{D2}}{\Delta_{D2}+\Omega_{E_2}}$ and $\Gamma_{\delta_3} = \frac{\Gamma_{11}+\Gamma_{41}}{2} + \frac{\Gamma_{11}\Delta_{D3}}{\Delta_{D3}+\Omega_{E_3}}$. These effective linewidths naturally give rise to the temporal correlation lengths between generated triphotons. Obviously, both the resonance centers and effective linewidths are velocity-dependent and subject to the Doppler broadening effect. From the calculated $\delta_{1\pm}$, $\delta_{2\pm\pm}$ and $\delta_{3\pm}$, we expect that there will be in general four sets of indistinguishable SSWM processes to produce time-energy-entangled W-triphotons. As a representative example, Fig. S2 presents $\chi^{(5)}$ under different scenarios. As one can see, after accomplishing the velocity integration, for the low OD, four distinct resonances will usually appear (see Figs. S2A and B); while for the high OD, it is possible to degenerate four resonances into two (see Fig. S2C).

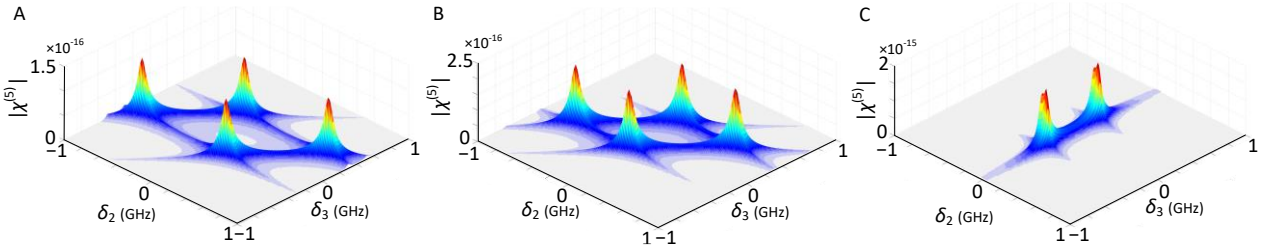

Fig. S2 | Representative illustration of the fifth-order nonlinear susceptibility $\chi^{(5)}$ under different parameter settings. (**A**) $\chi^{(5)}$ of **Fig. 2A** in the main text with the following simulation parameters: $\Gamma_{31} = \Gamma_{41} = 2\pi \times 6$ MHz, $\Gamma_{11} = \Gamma_{22} = 0.4 \times \Gamma_{41}$, $\Gamma_{21} = 0.2 \times \Gamma_{41}$, $\Delta_1 = -2$GHz, $\Delta_2 = -150$MHz, $\Delta_3 = 50$MHz, $OD = 4.6$, $\Omega_1 = 300$ MHz, $\Omega_2 = 870$ MHz, and $\Omega_3 = 533$ MHz for the input laser powers $P_1 = 4$ mW, $P_2 = 40$ mW, and $P_3 = 15$ mW. (**B**) $\chi^{(5)}$ of **Fig. 3A** in the main text with the same simulation parameters as (**A**) except $\Omega_2 = 533$ MHz, for the input power $P_2 = 15$ mW. (**C**) $\chi^{(5)}$ of **Fig. 3D** in the main text with the same simulation parameters as (**B**) except $OD = 45.7$.

Qualitative Derivations of Linear Susceptibilities χ

In addition to the resonance linewidths set by $\chi^{(5)}$, the triphoton temporal correlation is also dependent on the dispersion, which is determined by the linear optical response. After some calculations, the respective linear susceptibilities of the new E_{S1}, E_{S2} and E_{S3} fields are found to be

$$\chi_{S1} \approx 0, \tag{S3}$$

$$\chi_{S2} = \int f(v) \frac{-i4N\mu_{24}^2\left((1-\frac{v}{c})\delta_2 + i\Gamma_{22}\right)}{\varepsilon_0\hbar\left[4\left((1-\frac{v}{c})\delta_2 - \Delta_{D2} + i\Gamma_{42}\right)\left((1-\frac{v}{c})\delta_2 + i\Gamma_{22}\right) + |\Omega_2|^2\right]} dv, \tag{S4}$$

$$\chi_{S3} = \int f(v) \frac{-i4N\mu_{14}^2\left((1+\frac{v}{c})\delta_3 + i\Gamma_{11}\right)}{\varepsilon_0\hbar\left[4\left((1+\frac{v}{c})\delta_3 - \Delta_{D3} + i\Gamma_{41}\right)\left((1+\frac{v}{c})\delta_3 + i\Gamma_{11}\right) + |\Omega_3|^2\right]} dv. \tag{S5}$$

Eq. (S3) is well justified by the weak input E_1 beam and its associated large red detuning $\Delta_1 = -2$ GHz from the transition $|1\rangle \rightarrow |2\rangle$. This result indicates that the group velocity of the E_{S1} photons approximately coincides with the speed of light in vacuum, c. In Fig. S3, we have provided some

numerical simulations of χ_{S2} and χ_{S3} to show how their profiles look like. The group velocities experienced by the E_{S2} and E_{S3} photons can be routinely obtained by

$$v_{S2} = \left(\frac{dk_{S2}}{d\omega}\right)^{-1} = \frac{c}{1+\delta_2\left(\frac{dn_{S2}}{d\delta_2}\right)}, \tag{S6}$$

$$v_{S3} = \left(\frac{dk_{S3}}{d\omega}\right)^{-1} = \frac{c}{1+\delta_3\left(\frac{dn_{S3}}{d\delta_3}\right)}, \tag{S7}$$

where $n_{S2} = \sqrt{1 + \mathrm{Re}[\chi_{S2}]}$ and $n_{S3} = \sqrt{1 + \mathrm{Re}[\chi_{S3}]}$ are refractive indices. The imaginary parts of χ_{S2} and χ_{S3} tell the linear Raman gain or absorption undergone by the E_{S2} and E_{S3} photons when they traverse the medium. With these in mind, it is not difficult to compute the longitudinal phase mismatch in the SSWM process, which is

$$\Delta k(\delta_2, \delta_3) = k_{S1} - k_{S2} + k_{S3} - k_1 + k_2 - k_3, \tag{S8}$$

with $k_j = \bar{k}_j + \frac{\omega}{v_j} (j = 1,2,3,S1,S2,S3)$ and $\bar{k}_j$ the central wavenumber. Δk in Eq. (S8) gives the natural spectral width for the generated triphoton state. In other words, it naturally defines the temporal coherence time by means of the light propagation effect.

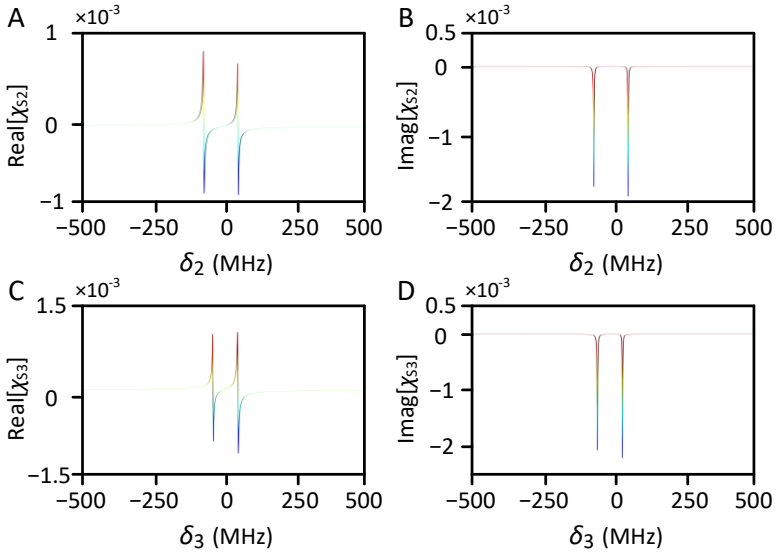

Fig. S3 | Representative examples of linear susceptibilities χ_{S2} and χ_{S3}. The involved parameters here are same as those employed in **Fig. S2B**. (**A & B**) The real and imaginary part of χ_{S2}. (**C & D**) The real and imaging part of χ_{S3}.

To get a sense how χ_{S2} and χ_{S3} behave, in Fig. S3 we use one example to qualitatively illustrate their real and imaginary parts after accomplishing the Doppler integration. As one can see, χ_{S2} and χ_{S3} are usually associated with two resonance structures as displayed in Figs. S3A–D. This is different from the four resonances of $\chi^{(5)}$ in Figs. S2A and B. This difference physically stems from the adopted qualitative model to calculate linear (and nonlinear) susceptibilities. Currently,

we are working on the exact theoretical calculations of both linear and nonlinear optical responses using the accurate model developed by Wen et al, and the results will be published elsewhere.

Derivation of the Triphoton State $|\Psi\rangle$

To calculate the three-photon state created from the SSWM process at the output surface of the medium, we shall work in the interaction picture and start with the effective Hamiltonian, which assumes the form of

$$H = \int_0^L dz \varepsilon_0 \chi^{(5)} E_1^{(+)} E_2^{(+)} E_3^{(+)} E_{S1}^{(-)} E_{S2}^{(-)} E_{S3}^{(-)} + H.c., \tag{S9}$$

where $H.c.$ means the Hermitian conjugate. The electric fields of the generated E_{S1}, E_{S2} and E_{S3} photons are described by the quantized fields,

$$E_{Sj}^{(+)} = \sum_{k_{Sj}} E_{Sj} a_j e^{i(k_{Sj} z - \omega_{Sj} t)}, \tag{S10}$$

where a_j is the annihilation operator for the mode with the wavenumber k_{Sj} and angular frequency ω_{Sj} and $E_{Sj} = i\sqrt{\hbar\omega_{Sj}/2\varepsilon_0 n_{Sj}^2 L}$. On the other hand, we take the three input lasers E_1, E_2 and E_3 to be classical plane waves,

$$E_1^{(+)} = E_1 e^{i(k_1 z - \omega_1 t)}, E_2^{(+)} = E_2 e^{i(-k_2 z - \omega_2 t)}, \text{ and } E_3^{(+)} = E_3 e^{i(k_3 z - \omega_3 t)}. \tag{S11}$$

The state vector of the triphotons can then be derived from first-order perturbation theory [1-17], which is

$$|\Psi\rangle = \frac{-i}{\hbar} \int_{-\infty}^{+\infty} dt H |0\rangle, \tag{S12}$$

with $|0\rangle$ being the initial vacuum state. By applying Eqs. (S9)–(S12) and retaining only the terms of interest, the triphoton state (S12) formally takes the form of

$$|\Psi\rangle = \sum_{k_{S1}} \sum_{k_{S2}} \sum_{k_{S3}} F(k_{S1}, k_{S2}, k_{S3}) \, a_{k_{S1}}^\dagger a_{k_{S2}}^\dagger a_{k_{S3}}^\dagger |0\rangle, \tag{S13}$$

where the three-photon spectral function F is defined as

$$F(k_{S1}, k_{S2}, k_{S3}) = A\chi^{(5)} \Phi(\Delta k L) \delta(\omega_1 + \omega_2 + \omega_3 - \omega_{S1} - \omega_{S2} - \omega_{S3}), \tag{S14}$$

with A being a grouped constant. In Eq. (S14), the Dirac δ function comes from the time integral in the steady-state approximation, and physically it assures the energy conservation in the SSWM process. From the viewpoint of atomic population, the energy conservation implies that after completing one triphoton generation, the population shall finish one cycle and return to its initial ground state $|1\rangle$. $\Phi(\Delta k L)$ is termed as the longitudinal phase-mismatch function and it has the form of

$$\Phi(\Delta kL) = \frac{1-e^{-i\Delta kL}}{i\Delta kL} = \mathrm{sinc}\left(\frac{\Delta kL}{2}\right) e^{-i\Delta kL/2}. \quad \text{(S15)}$$

Due to the Doppler effect in $\chi^{(5)}$ and Δk, it becomes generally difficult to have an exact analytical expression of the triphoton state (S13). Instead, hereafter we will resort to the numerical analysis on the triphoton properties.

Derivations of Temporal Correlation of W Triphotons

Optical properties of the W-type triphotons can be well understood by looking at the photon statistics through the photon-counting measurement. As such, we research the triphoton temporal correlation by calculating the Glauber second-order and third-order correlation functions. This in turn suggests us to investigate the conditioned two~photon coincidence counts and the three-photon coincidence counts.

In line with the experimental setup of Fig. 1 given in the main text, the averaged triphoton coincidence counting rate reads as

$$R_3 = \lim_{T\to\infty} \frac{1}{T} \int_0^T dt_1 \int_0^T dt_2 \int_0^T dt_3 \langle \Psi | E_{S1}^{(-)}(\tau_1) E_{S2}^{(-)}(\tau_2) E_{S3}^{(-)}(\tau_3) E_{S3}^{(+)}(\tau_3) E_{S2}^{(+)}(\tau_2) E_{S1}^{(+)}(\tau_1) | \Psi \rangle, \quad \text{(S16)}$$

and the two~photon coincidence counting rate is

$$R_2 = \lim_{T\to\infty} \frac{1}{T} \int_0^T dt_1 \int_0^T dt_2 \, \langle \Psi | E_{S2}^{(-)}(\tau_2) E_{S3}^{(-)}(\tau_3) E_{S3}^{(+)}(\tau_3) E_{S2}^{(+)}(\tau_2) | \Psi \rangle, \quad \text{(S17)}$$

by assuming the E_{s1} photons to be traced away for example. In Eqs. (S16) and (S17), $E_{Sj}^{(+)}(\tau_j)$ $(j = 1,2,3)$ is the positive frequency part of the free-space electric field evaluated at the jth detector's spatial coordinate r_j and trigger time t_j with $\tau_j = t_j - r_j/c$. For the sake of simplicity, we take the efficiencies of all single-photon detectors to be unity. On the other hand, the narrow bandwidths (less than GHz) of the triphotons considered here are comparable to or smaller than the spectral width of the employed single-photon detectors in our experiment. We thus can simplify Eqs. (S16) and (17) to

$$R_3 = \left| \langle 0 | E_{S3}^{(+)}(\tau_3) E_{S2}^{(+)}(\tau_2) E_{S1}^{(+)}(\tau_1) | \Psi \rangle \right|^2 = |A_3(\tau_1, \tau_2, \tau_3)|^2, \quad \text{(S18)}$$

$$R_2 = \sum_{k_{S1}} \left| \langle 0 | a_{k_{S1}} E_{S3}^{(+)}(\tau_3) E_{S2}^{(+)}(\tau_2) | \Psi \rangle \right|^2 = \sum_{k_{S1}} |A_2(\tau_2, \tau_3)|^2, \quad \text{(S19)}$$

where $A_3(\tau)$ is often referred to as the three-photon amplitude or the triphoton waveform. It is worth to emphasize that $A_2(\tau)$ is also the three-photon amplitude, despite one subsystem is not detected in the experiment. Note that both $A_3(\tau)$ and $A_2(\tau)$ are defined with reference to the photon detections. Plugging Eq. (S13) into Eq. (S18) yields

$$A_3(\tau_1,\tau_2,\tau_3) = A_3 \sum_{k_{S1}} \sum_{k_{S2}} \sum_{k_{S3}} e^{-i(\omega_{S1}\tau_1+\omega_{S2}\tau_2+\omega_{S3}\tau_3)} F(k_{S1},k_{S2},k_{S3}). \quad \text{(S20)}$$

Again, all slowly varying terms and constants have been absorbed into A_3. Similarly, substituting Eq. (S13) into Eq. (S19) gives

$$A_2(\tau_2,\tau_3) = A_2 \sum_{k_{S2}} \sum_{k_{S3}} e^{-i(\omega_{S2}\tau_2+\omega_{S3}\tau_3)} F(k_{S1},k_{S2},k_{S3}), \quad \text{(S21)}$$

where all the slowly varying terms and constants have been grouped into A_2, too. Additionally, to evaluate the Dirac δ function in F (S14), we will replace the summation over a wavenumber by an angular frequency integral as usual,

$$\sum_{k_{Sj}} \to \frac{L}{2\pi} \int d\omega_{Sj} \frac{dk_{Sj}}{d\omega_{Sj}} = \frac{L}{2\pi} \int \frac{d\omega_{Sj}}{v_{Sj}}. \quad \text{(S22)}$$

With use of Eqs. (S13) and (S22), the three-photon amplitude (S20) then becomes

$$A_3(\tau_{21},\tau_{31}) = A_3 \int\int d\delta_2 d\delta_3 \, \chi^{(5)}(\delta_2,\delta_3) \mathrm{sinc}\left[\frac{\Delta k(\delta_2,\delta_3)L}{2}\right] e^{-i\delta_2(\tau_{21}+L/2v_{S2})} e^{-i\delta_3(\tau_{31}+L/2v_{S3})}. \quad \text{(S23)}$$

The three-photon coincidence counting rate (S18) is simply module squared of $A_3(\tau_{21},\tau_{31})$, i.e.,

$$R_3 = |A_3(\tau_{21},\tau_{31})|^2.$$

From Eq. (S23), it is not difficult to see that the three-photon amplitude $A_3(\tau_{21},\tau_{31})$ is the convolution of the fifth-order nonlinear susceptibility $\chi^{(5)}(\delta_2,\delta_3)$ and the longitudinal phase-mismatch function $\Phi(\Delta kL)$. Physically, this implies that the triphoton temporal coherence is jointly determined by these two factors. As a consequence, two distinct regions can be expected to appear in three-photon temporal correlation measurements, the so-called damped Rabi oscillation regime dominated by $\chi^{(5)}$ and the group-delay regime dominated by $\Phi(\Delta kL)$. We have examined these regions in the experiment and presented some recorded data in Figs. 2–4 in the main text as well as Figs. S11 and S12 below. As a qualitative comparison, in Fig. S4 we have provided their corresponding theoretical simulations. It is easy to see that both Figs. S4A and B exhibit the three-photon coincidence counts in the damped Rabi oscillation regime, while Fig. S3C displays the case in the group-delay region, which qualitatively explain the experimental observations of Figs. 2A, 3A and 3D in the main text.

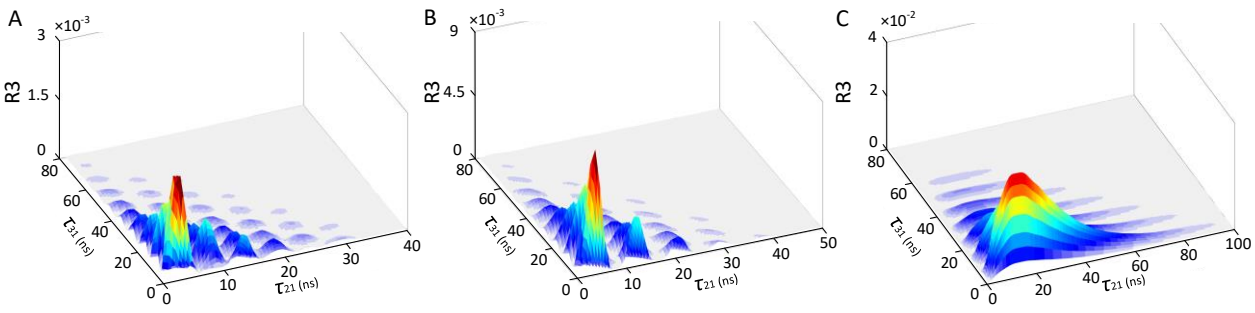

Fig. S4 | Theoretical simulations of triphoton coincidence counting rates R_3. (**A**) R_3 corresponding to **Fig. 2A** in the main text with the same parameters used in **Fig. S2A**. (**B**) R_3 corresponding to **Fig. 3A** in the main text with the same parameters used in **Fig. S2B**. (**C**) R_3 corresponding to **Fig. 3D** in the main text with the same parameters used in **Fig. S2C**.

In the similar way, we can show that the conditioned two~photon coincidence counting rate can be evaluated by

$$R_2(\tau_{23}) = R_2 \int d\delta_3 \left| \int d\delta_2 \, \chi^{(5)}(\delta_2, \delta_3) \mathrm{sinc}\left[\frac{\Delta k(\delta_2,\delta_3)L}{2}\right] e^{-i\delta_2(\tau_{23}+L/2v_{S2})} \right|^2, \tag{S24}$$

where $\tau_{23} = \tau_2 - \tau_3$ and R_2 is a grouped constant. As one can see from Eq. (S24), $R_2(\tau_{23})$ is a function of τ_{23}, implying the existence of a partial entanglement between the remaining E_{S2} and E_{S3} photons after tracing the E_{S1} photon away. This is clearly a signature of the property of the tripartite W class. In Eq. (S24), the second integral inside the module squared is a convolution between $\chi^{(5)}$ and $\Phi(\Delta kL)$. Similarly, the functional profile of $R_2(\tau_{23})$ is in general determined by both factors. However, if either of them plays the dominant role, $R_2(\tau_{23})$ will showcase two distinctive scenarios, the damped Rabi oscillation regime and the group-delay regime. Other arrangements on conditional two~photon coincidence counts can be calculated by following the same reasoning. Here, we will not repeat those calculations and leave them as an exercise to the reader. In Figs. 2C and D and Figs. 3B, C, E and F in the main text, we have reported examples of such measured conditional two~photon coincidence counts. As a comparison, Fig. S5 accordingly presents their respective theoretical simulations. As one can see, our theory qualitatively agrees with the experiment.

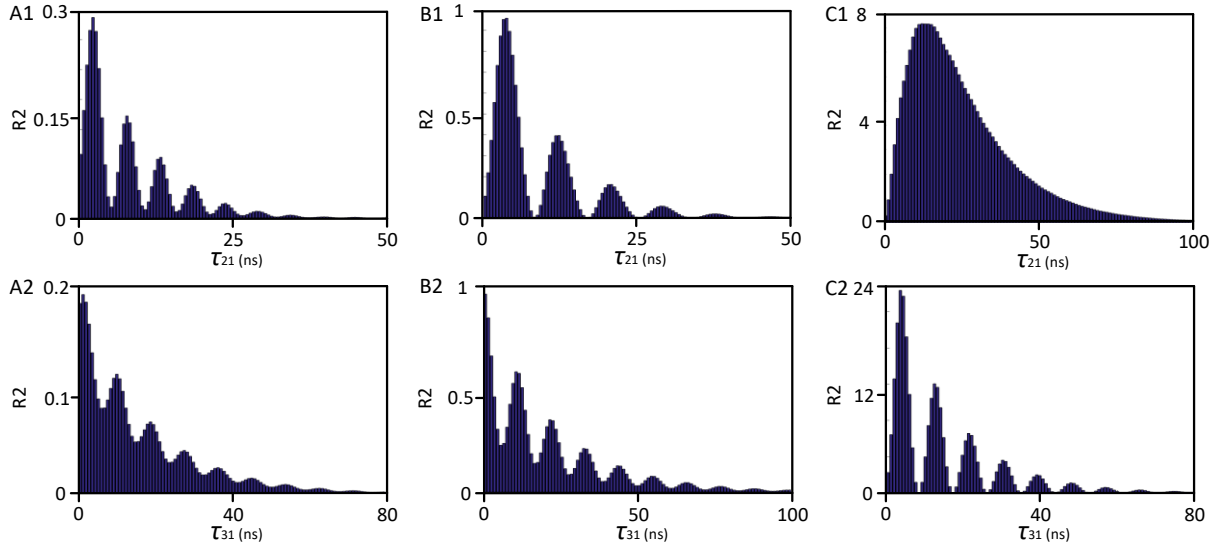

Figure S5 | Theoretical simulations of conditional two~photon coincidence counting rates R_2 for Fig. S4. (**A1**) R_2 by tracing the E_{S3}-photons away in **Fig. S4A**. (**A2**) R_2 by tracing the E_{S2}-photons away in **Fig. S4A**. (**B1**) R_2 by tracing the E_{S3}-photons away in **Fig. S4B**. (**B2**) R_2 by tracing the E_{s2}-photons away in **Fig. S4B**. (**C1**) R_2 by tracing the E_{S3}-photons away in **Fig. S4C**. (**C2**) R_2 by tracing the E_{S2}-photons away in **Fig. S4C**.

Triphoton W State Entangled in Other Degrees of Freedom

Although the focus of the current work is on time-energy-entangled W triphotons, in fact, they can be also entangled in other degrees of freedom including space-momentum, polarization, and orbital angular momentum. Thanks to the SSWM process vastly enhanced by atomic coherence, it allows one to explore various three-photon entanglement based on different degrees of freedom, which becomes uneasy or even impossible to achieve with previously proposed schemes or methods. Moreover, our system is capable of forming triphoton hyperentangled states by entangling more than one degree of freedom of light, which will become technically challenging for any previously reported multiphoton generation platform. The system layouts and theoretical calculations on these triphoton entangled states are out of the scope of the present work and will be discussed elsewhere. Of importance, triphotons entangled in different degrees of freedom promise distinctive quantum technological applications. For instance, the W-type triphotons with spatial correlations [19-21] can be used to achieve quantum imaging and remote sensing with sub-Rayleigh superresolution that cannot be mimicked and even accessed by biphotons or classical light, thereby making the whole phenomena indisputably quantum.

II. Further Information on Experimental Measurements and Data Processing

In what follows, we would like to provide further details on the experimental measurements and data processing. We will also report more recorded experimental data on triphoton coincidences to demonstrate that, indeed, the proposed SSWM in coherent atomic ensembles is an efficient process to yield high-quality and reliable genuine triphotons. Of importance, these data plus those in the main text give a good account of the versatility of the source, which may enable new technological developments unreachable to the current photon resources.

Possible Biphoton Processes

As mentioned in the Methods, one major accidental coincidence noise in three-photon correlation measurement comes from the simultaneous presence of two pairs of biphotons, from different spontaneous four-wave mixing (SFWM) processes, onto the single-photon detectors. Fortunately, these SFWMs are accompanied by different phase matching conditions, deviating from the one for the SSWM process. Moreover, the biphotons originating from these SFWMs have different central frequencies from those of the desired triphotons. As such, by carefully manipulating the phase matching conditions and employing narrowband filters, one can effectively remove these biphoton false trigger events from the genuine triphoton coincidence counts. To have an intuitive picture of these biphoton generations, in Fig. S6 we have schematically illustrated all possible SFWM processes. According to the level structure, we have identified seven such SFWM processes and depicted them in Figs. S6B–H**.** The biphotons produced from these SFWMs are the main source of accidental coincidences to the real measurements. In Methods, we have already elaborated on their possible combinations for potential error-triggering events.

Although entangled quadraphotons might be generated from a higher-order nonlinear wave mixing process, their emission possibility will be sufficiently low and won't become one major noise source to the triphoton detection. As such, we won't discuss them here further.

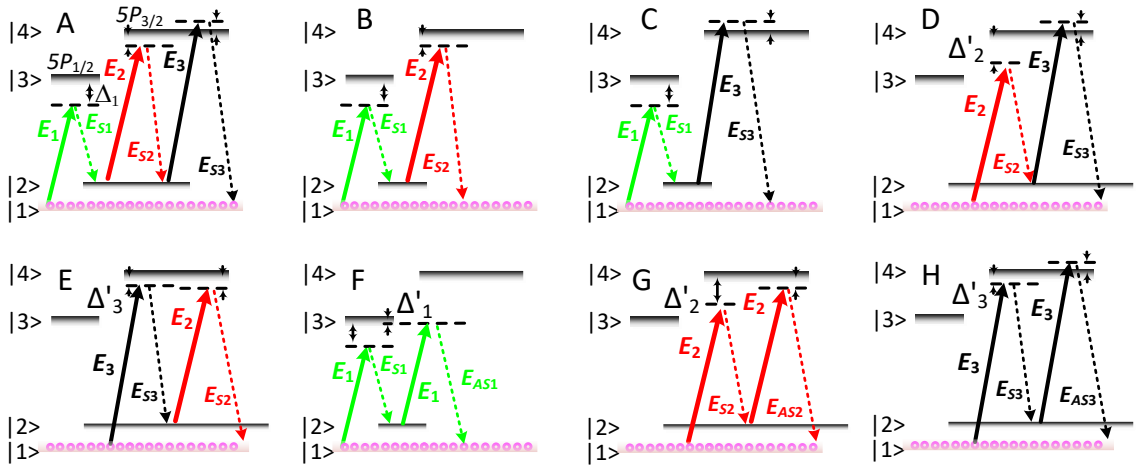

Figure S6 | Seven possible SFWM processes which may result in accidental coincidences onto three-photon coincidence counting measurement. (**A**) Atomic energy-level structure for triphoton generation. (**B-H**) Seven possible SFWM processes where the emitted biphotons may become accidental coincidences in the measured three-photon coincidence counts.

Measured Coincidence Counts by Subtracting Background Accidentals

In Figs. 2 and 3 in the main text, we have presented the recorded data with background accidental counts. Here, in Fig. S7 and S8, we have processed these measured data by subtracting these background accidental counts. By comparing Figs. 2 and 3 with Fig. S7 and S8, one can see that the essential features have been well retained for both cases. In Figs. S7C, S7D, S8B, S8C and S8F, we have illustrated the oscillation periods mentioned in the main text with green and red dashed lines based on the measured data. By comparing Figs. S7C, S7D, S8B, S8C, S8E and S8F with Figs. S4A1–C2, we are aware that our qualitative mode on optical response can only provide a qualitative interpretation to the experimental results. But nevertheless, it does reveal certain key features of the measurements.

To gain a better understanding of the conditional two~photon coincidences and conditional three-photon coincidences, we have further processed the experimental data in Figs. 2A, 3A and 3D by looking at other different scenarios after removing the corresponding background accidental counts. As some typical examples, Fig. S9 reports a portion of such processed experimental data in a way by complying with specific conditions. From these figures, it is not difficult to find that the coherence length of the two~photon residual temporal correlation is not fixed and depends on the conditions of the performed measurement. This is also applicable to the coherence length of the conditional three-photon temporal correlation. All in all, these features are not available from the previous demonstrations. From another point of view, this also proves that the generated three-photon state has flexible and tunable characteristics, which are essential for its various applications.

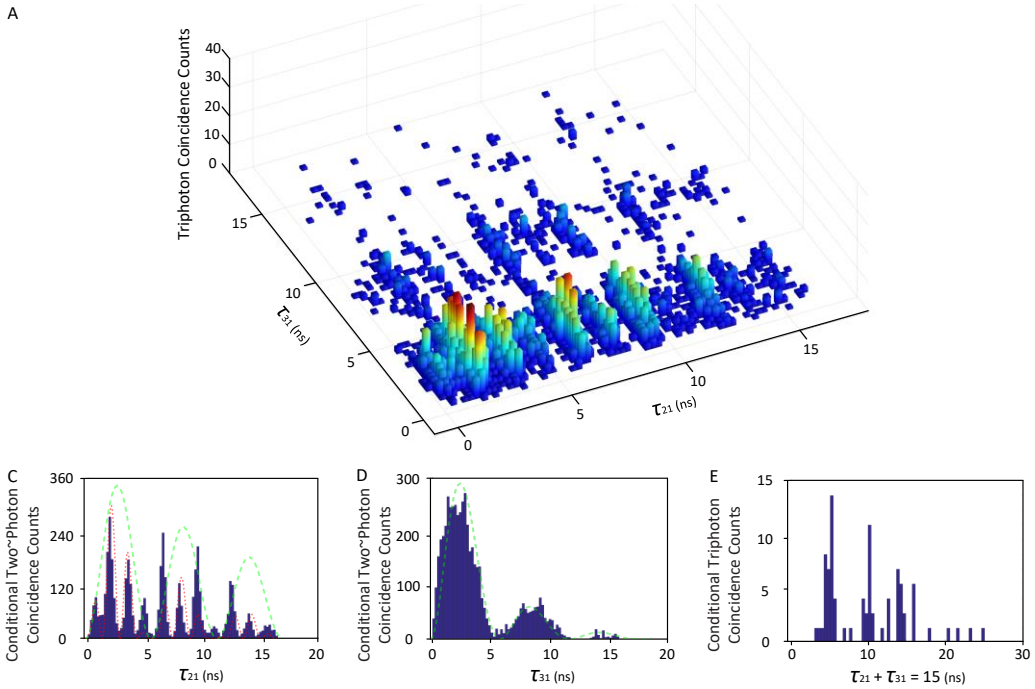

Fig. S7 | Triphoton coincidence counts, conditioned two~photon coincidence counts, and conditional three-photon coincidence counts presented in Fig. 2 in the main text by removing background accidentals. In (**C & D**), the green and red dashed lines are used to illustrate periodic oscillations mentioned in the main text.

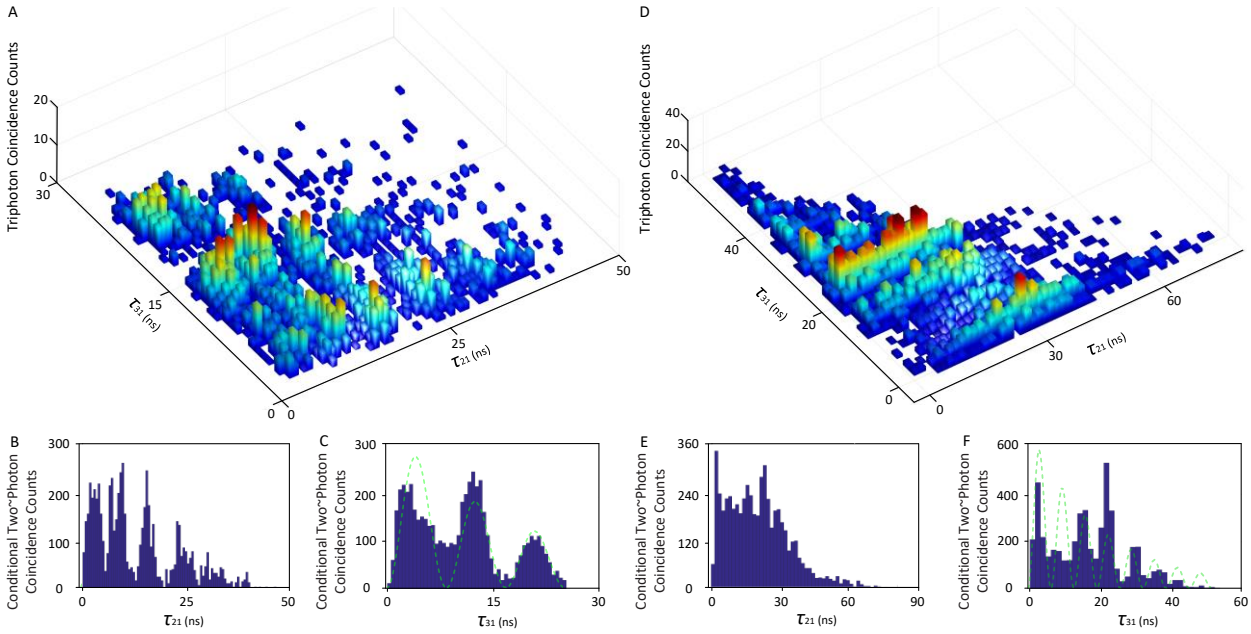

Fig. S8 | Triphoton coincidence counts, conditioned two~photon coincidence counts, and conditional three-photon coincidence counts displayed in Fig. 3 in the main text by subtracting background accidentals. In (**B, C & F**), the green dashed lines are used to illustrate periodic oscillations mentioned in the main text.

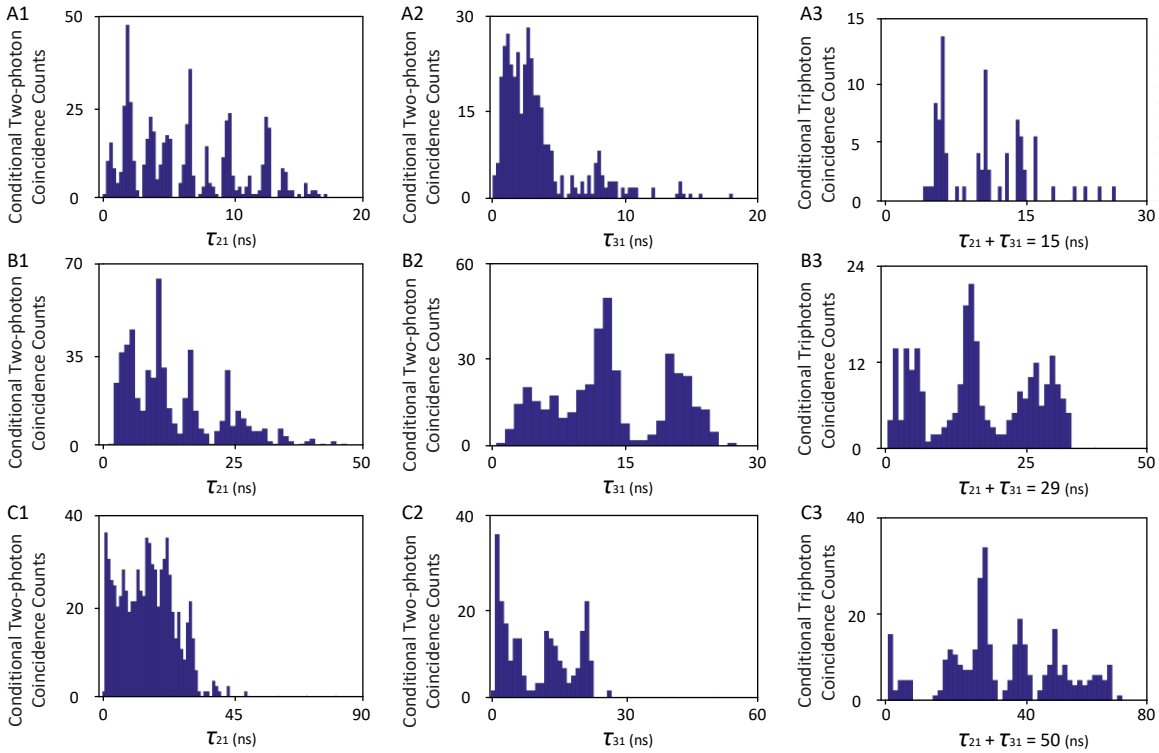

Fig. S9 | Conditional two~photon coincidence counts R_2 and conditional triphoton coincidence counts R_3 by subtracting their respective background accidentals for the scenarios of Figs. 2A, 3A and 3D shown in the main text. Specifically, (**A1**) $R_2(\tau_{21})$ by fixing $\tau_{31} = 2.6$ ns for R_3 in **Fig. 2A** in the main text; (**A2**) $R_2(\tau_{31})$ by fixing $\tau_{21} = 2.0$ ns for R_3 in **Fig. 2A**; (**A3**) $R_3(\tau_{21} + \tau_{31} = 15.0$ ns) for R_3 in **Fig. 2A**; (**B1**) $R_2(\tau_{21})$ by fixing $\tau_{31} = 13.0$ ns for R_3 in **Fig. 3A** in the main text; (**B2**) $R_2(\tau_{31})$ by fixing $\tau_{21} = 4.0$ ns for R_3 in **Fig. 3A**; (**B3**) $R_3(\tau_{21} + \tau_{31} = 29.0$ ns) for R_3 in **Fig. 3A**; (**C1**) $R_2(\tau_{21})$ by fixing $\tau_{31} = 21.0$ ns for R_3 in **Fig. 3D** in the main text; (**C2**) $R_2(\tau_{31})$ by fixing $\tau_{21} = 31.0$ ns for R_3 in **Fig. 3D**; (**C3**) $R_3(\tau_{21} + \tau_{31} = 50.0$ ns) for R_3 in **Fig. 3D**.

Reconstruction Procedure for Triphoton Coincidence Counts

Unlike the standard two-photon correlation measurement, in practice, no generic three-photon coincidence circuit is commercially available in the market. As a result, each group has to build up its own three-photon coincidence circuit. As laid out in Fig. S10, we construct such a detection system based on two-photon coincidence circuits. Specifically, in a preset three-photon correlation time window, we reconstruct three collected single-photon trigger events from $SPCM_1$, $SPCM_2$ and $SPCM_3$ through the simultaneous detection of two pairs of two-photon coincidence counts, $\{E_{S1}, E_{S2}\}$ and $\{E_{S1}, E_{S3}\}$, with the help of an additional diagnose $SPCM_D$. In the experiment, for every recorded three-photon coincidence count, we use the E_{S1}-photon click as a shared start trigger to initiate two electronic pulses I_1 from $SPCM_1$, one of which undergoes a 150-ns delay, as shown in Fig. S10A. Meantime, the detections of the E_{S2}- and E_{S3}-photon will jointly serve as the stop trigger, where the electronic pulse I_3 from $SPCM_3$ will be delayed by 150 ns with respect to the electronic pulse I_2 from $SPCM_2$. With these arrangements, the E_{S1} and E_{S2} photons will be measured first as a function of τ_{21}, and then the E_{S1} and E_{S3} photons will be recorded after 150 ns

as a function of τ_{31}. In this way, the three-photon temporal correlations can be captured in the coincidence counting measurement. To see how each two-photon coincidence counting component works, in Fig. S10B–D we have presented one set of such experimental data collected over 5 minutes by setting the time bin width of each SPCM to be 0.25 ns. As one can see, the joint detection of the E_{S1} and E_{S2} photons gives rise to two~photon temporal correlation as a function of the relative time difference τ_{21} between the clicks of the two involved single-photon detectors, $SPCM_1$ and $SPCM_2$ (see Fig. S10B). Similarly, the joint detection of the E_{S1} and E_{S3} photons reveals their residual temporal correlation as a function of the relative triggering time difference τ_{31} between the clicks of the two involved single-photon detectors $SPCM_1$ and $SPCM_3$ (see Fig. S10C). Since the diagnose single-photon detector $SPCM_D$ is triggered by artificial electronic signals, the coincidence counting detection between the E_{S3} photons and artificial diagnose signals will result in no exact temporal correlation as reflected in Fig. S10D.

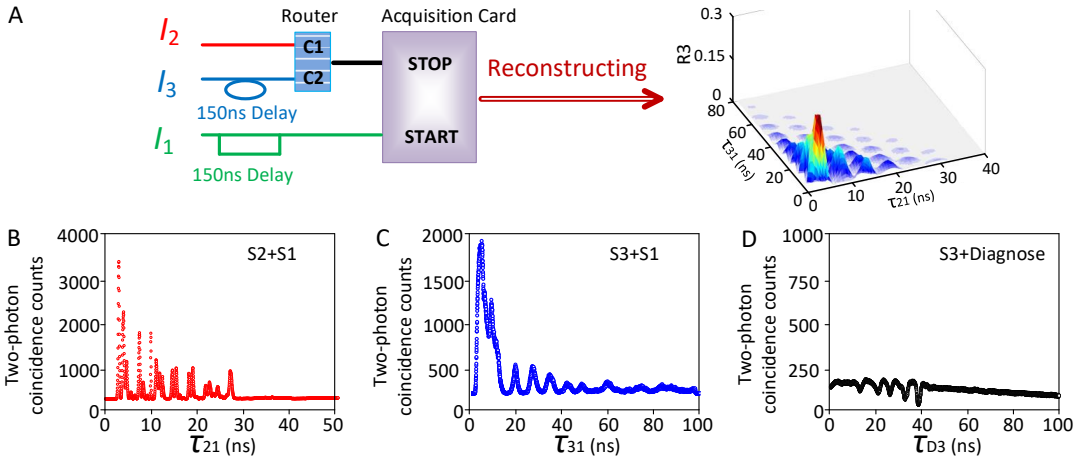

Fig. S10 | Three-photon detection system and coincidence counting reconstruction. (**A**) Schematic of our home-made detection system enabling three-photon coincidence counting reconstruction. As an example, (**B–D**) exhibit the recorded two-photon coincidence counts in one experiment, respectively, by $SPCM_1$ and $SPCM_2$, $SPCM_1$ and $SPCM_3$, and $SPCM_3$ and $SPCM_D$ as functions of the relative time differences τ_2, τ_3 and τ_d between the clicks of the two involved single-photon detectors. The experimental data was collected over 5 minutes by setting the bin width of each SPCM to 0.25 ns. Other parameters are $P_1 = 4$ mW, $P_2 = 40$ mW, $P_3 = 15$ mW, $\Delta_1 = -2$GHz, $\Delta_2 = -150$MHz, $\Delta_3 = 50$MHz, $\Omega_1 = 300$ MHz, $\Omega_2 = 870$ MHz, $\Omega_3 = 533$ MHz.

Experimentally, to catch genuine triphotons in detection, it is very important to optimize the phase-matching conditions of the SSWM process by controlling the wavelengths and injection angles of three input optical driving beams as well as the triphoton collection directions. Other than these arrangements, to ensure that the detected triphotons indeed come from the desired SSWM process, we have further implemented an additional coincidence counting detection by jointly measuring the E_{S3} photons with the artificially introduced diagnose signals from $SPCM_D$ in simultaneous conjunction with the joint detection of the E_{S1} and E_{S2} photons. By applying the same reconstruction method described above, we have obtained only a few accidental coincidences per

minute when using the two-photon coincidences $\{E_{S1}, E_{S2}\}$ and $\{E_{S3}, E_D\}$ to construct the three-photon histogram, indicating that, indeed, no true quantum correlation shall exist in any two pairs of uncorrelated two-photon coincidences.

Additional Experimental Data

In the experiment, we have carried out a series of three-photon coincidence counting measurements by changing the system parameters. In addition to the data illustrated in Figs. 2 and 3 in the main text, here we would like to show another group of measured data. As plotted in Fig. S11, we collected the three-photon coincidence trigger events over 1 h with the time bin width of each SPCM to be set at 2.0 ns. Most of the experimental parameters are same as those of Fig. 2A in the main text except $P_2 = 7$ mW, $P_3 = 7$ mW, and $OD = 45.7$. According to the recorded data, we found that the triphoton production rate is 100 ± 11 per minute but with the background accidentals of 8 ± 3.1 per minutes. Also in such a case, the triphoton temporal correlation falls into the group-delay regime. This can be well verified by examining the conditional two~photon correlations by tracing either one photon away from every triphoton. In Fig. S11B and C, we have presented such conditional two~photon coincidence counts. As one can see, the Rabi oscillations almost disappear in these two figures.

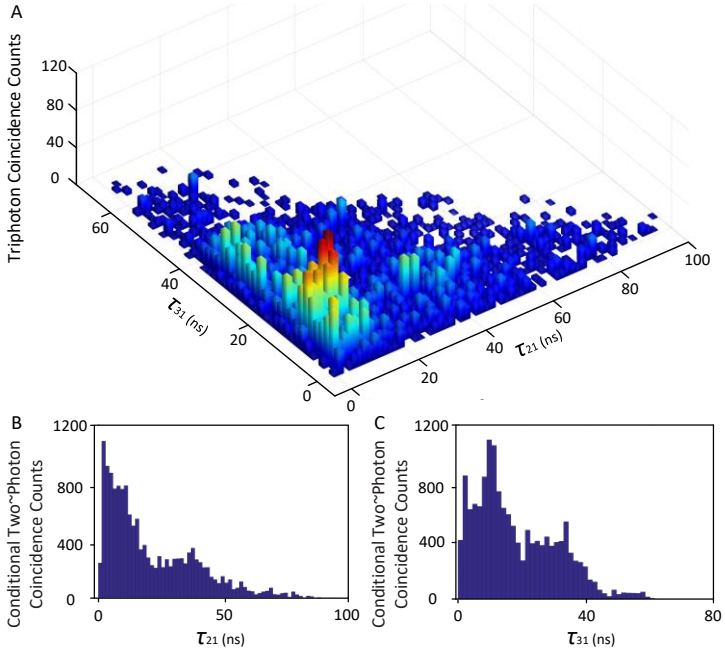

Fig. S11 | Triphoton temporal correlation in the group-delayed region. (**A**) The histogram of three-photon coincidence counts over 1 hour with 2.0-ns time-bin width for each single-photon detector. The triphoton overall generation rate reads as 100 ± 11 per minute with the measured background accidental coincidences to be 8 ± 3.1 per minute. (**B & C**) Conditional two~photon coincidence counts by tracing the E_{S3} or E_{S2} photons away from each three-photon joint trigger event in (**A**). The experimental parameters are same as those of **Fig. 2A** in the main text except for $P_2 = 7$ mW, $P_3 = 7$ mW, $\Omega_2 = 364$ MHz, $\Omega_3 = 364$ MHz, and $OD = 45.7$.

In Fig. S12, we have reported another set of measurements in the group-delay region. In comparison to Fig. S11, one can see that the small oscillations in the previous figures are largely suppressed.

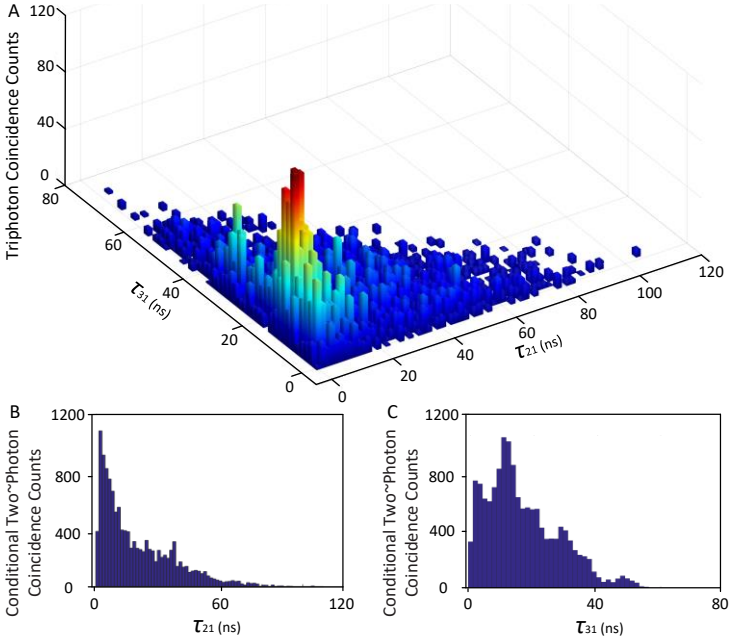

Fig. S12 | Triphoton temporal correlation in the group-delayed region. (**A**) The histogram of three-photon coincidence counts over 1.5 hours with 1.5-ns time bin width for each single-photon detector. The triphoton overall generation rate reads as 140 ± 15 per minute with the measured background accidental coincidences to be 13 ± 3.4 per minute. (**B & C**) Conditional two~photon coincidence counts by tracing the E_{S3} or E_{S2} photons away from each three-photon joint trigger event in (**A**). The experimental parameters are same as those of **Fig. 2A** in the main text except for $P_2 = 6$ mW, $P_3 = 6$ mW, $\Omega_2 = 351$ MHz, $\Omega_3 = 351$ MHz, and $OD = 45.7$.

III. Comparison of Various Mechanisms on Multiphoton Generation

In this session, we have summarized most of the major experimental demonstrations on entangled three-photon and multi-photon generation reported so far, and have tabulated their critical parameters and achieved optical properties in TABLE I for comparison.

Degree of freedom	Counts per hour	Class	Year (reference)
Path	24	3-photon GHZ	*Phys. Rev. Lett.* **82**, 1345-1349 (1999)
Path	69	4-photon GHZ	*Phys. Rev. Lett.* **86**, 4435-4439 (2001)
Path	3600	4-photon Dicke	*Phys. Rev. Lett.* **98**, 063604 (2007)
Energy-time	6.2±0.55	3-photon	*Nature* **466**, 601-603 (2010)

Energy-time	7	3-photon	*Nat. Phys*. **9**, 19-22 (2013)
Polarization	744±150	3-photon	*Nat. Photon.* **8**, 801-807 (2014)
Path	10	5-photon	*Nature* **430**, 54-58 (2004)
Polarization	5220	3-photon W	*Phys. Rev. Lett.* **95**, 150404 (2005)
Polarization	300	4-Photon	*Phys. Rev. Lett.* **90**, 200403 (2003)
Polarization	175	4-Photon	*Phys. Rev. Lett.* **92**, 107901 (2004)

IV. Further Discussion on the Reported Triphoton Source

It is instructive to look at whether the reported triphoton source would be able to produce the GHZ-type triphotons entangled in time-energy (and other degrees of freedom) [22,23]. To the best of our knowledge, so far there is no single proposal on direct generation of continuous-mode time-energy-entangled GHZ triphotons in the literature. This is due to the fact that, in order to create such a three-photon GHZ state, two of them must be degenerate in every degree of freedom [22]. For our triphoton source, you might be wondering what if two of them are arranged into a degenerate state, would we form a GHZ state? In theory, this is viable. But technically, an experiment of such will be highly challenging.

References

[1] Wen, J., Du, S. & Rubin, M. H. Biphoton generation in a two-level atomic ensemble. *Phys. Rev. A* **75**, 033809 (2007).

[2] Wen, J., Du, S. & Rubin, M. H. Spontaneous parametric down-conversion in a three-level system. *Phys. Rev. A* **76**, 013825 (2007).

[3] Wen, J., Du, S., Zhang, Y., Xiao, M. & Rubin, M. H. Nonclassical light generation via a four-level inverted-Y system. *Phys. Rev. A* **77**, 033816 (2008).

[4] Zhang, D., Cai, Y., Zheng, Z., Barral, D., Zhang, Y., Xiao, M. & Bencheikh, K. Non-Gaussian nature and entanglement of spontaneous parametric nondegenerate triple-photon generation. *Phys. Rev. A* **103**, 013704 (2021).

[5] Li, K., Cai, Y., Wu, J., Liu, Y., Xiong, S., Li, Y. & Zhang, Y. Three-body topology entanglement generation via a six-wave mixing: Competing and coexisting of linear and nonlinear optical responses in triphoton temporal correlation. *Adv. Quantum Technol.* **3**, 1900119 (2020).

[6] Nie, Z., Zheng, H., Li, P., Yang, Y., Zhang, Y. & Xiao, M. Interacting multiwave mixing in a five-level atomic system. *Phys. Rev. A* **77**, 063829 (2008).

[7] Chen, H. X., Qin, M. Z., Zhang, Y. Q., Zhang, X., Wen, F., Wen, J. & Zhang, Y. Parametric amplification of dressed multi-wave mixing in an atomic ensemble. Laser. Phys. Lett. 11, 045201 (2014).

[8] Li, K., Zhang, D., Raza, F., Zhang, Z., Puttapirat, P., Liu, Y. & Zhang, Y. Multi-contact switch using double-dressing regularity of probe, fluorescence, and six-wave mixing in a Rydberg atom. *J. Chem. Phys.* **149**, 074310 (2018).

[9] Wen, J., Oh, E. & Du, S. Tripartite entanglement generation via four-wave mixings: narrowband triphoton W state. *J. Opt. Soc. Am. B* **27**, A11-A20 (2010).

[10] Yun, S., Wen, J., Xu, P., Xiao, M. & Zhu, S. N. Generation of frequency-correlated narrowband biphotons from four-wave mixing in cold atoms. *Phys. Rev. A* **82**, 063830 (2010).

[11] Wen, J., Zhai, Y. H., Du, S. & Xiao, M. Engineering biphoton wave packets with an electromagnetically induced grating. *Phys. Rev. A* **82**, 043814 (2010).

[12] Du, S., Wen, J. & Rubin, M. H. Narrowband biphoton generation near atomic resonance. *J. Opt. Soc. Am. B* **25**, C98-C108 (2008).

[13] Du, S., Oh, E., Wen, J. & Rubin, M. H. Four-wave mixing in three-level systems: Interference and entanglement. *Phys. Rev. A* **76**, 013803 (2007).

[14] Du, S., Wen, J., Rubin, M. H. & Yin, G. Y. Four-wave mixing and biphoton generation in a two-level system. *Phys. Rev. Lett.* **98**, 53601 (2007).

[15] Wen, J. & Rubin, M. H. Transverse effects in paired-photon generation via an electromagnetically induced transparency medium. I. Perturbation theory. *Phys. Rev. A* **74**, 023808 (2006).

[16] Keller, T. E., Rubin, M. H., Shih, Y. & Wu, L.-A. Theory of the three-photon entangled state. *Phys. Rev. A* **57**, 2076-2079 (1998).

[17] Rubin, M. H., Klyshko, D. N., Shih, Y.-H. & Sergienko, A. V. Theory of two-photon entanglement in type-II optical parametric down-conversion. *Phys. Rev. A* **50**, 5122-5133 (1994).

[18] Klyshko, D. N. *Photons and Nonlinear Optics* (Gordon and Breach, 1988).

[19] Wen, J., Xu, P., Rubin, M. H. & Shih, Y. Transverse correlation in triphoton entanglement: Geometrical and physical optics. *Phys. Rev. A* **76**, 023828 (2007).

[20] Wen, J., Rubin, M. H. & Shih, Y. Transverse correlation in multiphoton entanglement. *Phys. Rev. A* **76**, 45802 (2007).

[21] Wen, J., Du, S. & Xiao, M. Improving spatial resolution in quantum imaging beyond the Rayleigh diffraction limit using multiphoton W entangled states. *Phys. Lett. A* **374**, 3908-3911 (2010).

[22] Wen, J. & Rubin, M. H. Distinction of tripartite Greenberger-Horne-Zeilinger and W states entangled in time (or energy) and space. *Phys. Rev. A* **79**, 025802 (2009).

[23] Wen, J., Rubin, M. H. & Shih, Y. H. Spatial resolution enhancement in quantum imaging beyond the diffraction limit using entangled photon-number state. arXiv:0812.2032 (2008).